Solid State Sciences 157 (2024) 107719

Contents lists available at ScienceDirect

Solid State Sciences

journal homepage: www.elsevier.com/locate/ssscie

$La_2O_2MQ_2$ phases: Stability and synthetic challenges

Glen R. Hebberd, Budhika G. Mendis, Leon Bowen, Stewart J. Clark, Emma E. McCabe *

Department of Physics, Durham University, South Road, Durham, DH1 3LE, UK

A B S T R A C T

Oxychalcogenides containing transition metal or p block cations have potential for thermoelectric, photocatalytic and magnetic applications but the synthetic pathways to these quaternary phases are not fully understood. This presents a challenge to the design and preparation of new functional materials. Our combined experimental and computational study of $La_2O_2MQ_2$ (M = +2 cation; Q = sulfide, selenide anion) systems explores the thermodynamic constraints on synthesis and highlights the subtle balance in stabilities of phases formed via competing reaction pathways.

1. Introduction

Designing functional materials to meet the demands of current innovations is challenging and often requires complex combinations of physical properties, such as the high electrical conductivity and low thermal conductivity for thermoelectrics [4], or specific symmetry and band gap requirements for new photovoltaics [5] and photocatalysts [6]. The opportunities offered by mixed-anion materials have motivated researchers to explore more diverse compositions and the additional degrees of freedom from multiple anions can tune the structure and symmetry, the band gap and therefore physical properties [7,8]. This makes for exciting opportunities in functional materials design, but also presents difficulties in preparing these materials; the synthetic routes to these, often metastable, phases, are not as well understood as for oxides and other homo-anionic materials. Oxychalcogenides, containing both oxide (O^{2-}) as well as larger sulfide, selenide or telluride (S^{2-}, Se^{2-} or Te^{2-}) anions are gaining increased attention for their thermoelectric [3,9], non-linear optical [10,11] and photocatalytic properties [12–14]. Recent research has highlighted new synthesis routes [1,15,16] prompting us to explore the synthesis of some M^{2+} oxychalcogenides in this work. Our initial motivation was to explore oxysuflides containing ns^2 lone pair cations (such as $5s^2$ Sn^{2+} and Sb^{3+} cations), given the promising electronic structure of several Sb^{3+} containing phases for possible photocatalytic applications [17–20]. This led us to consider the electronic structure of several Sn^{2+} oxysulfides for possible photocatalytic applications (see supporting information) and their synthesis, alongside analogues containing the $3d^{10}$ Zn^{2+} cation for comparison.

The difference in size and charge between the oxide and sulfide/selenide/telluride anions favours anion-ordered structures for many oxychalcogenides which are often layered [3,21]. A frequently observed structural motif in this family is the fluorite-like $[Ln_2O_2]^{2+}$ layer, composed of edge-linked OLn_4 tetrahedra [22], as found in the ZrCuSiAs structure, adopted by thermoelectric BiCuOSe [23–25] (and related phases [26,27] including LaCuOS [28]) and the isostructural iron oxyarsenides known for their superconductivity, as illustrated in Fig. 1 [29,30]. Oxychalocgenides of general formula $Ln_2O_2MQ_2$ (Q = S, Se) containing M^{2+} cations can adopt ZrCuSiAs-derived structures with half-occupied cation sites within the anti-fluorite-like M – Q layers. These cation sites may be occupied in a disordered fashion (as originally reported for $CeOMn_{0.5}Se$) [31], or might order in a checkerboard arrangement (Fig. 1b) [32–34], into stripes (Fig. 1d) [35,36], or an intermediate structure containing both checkerboard and stripe fragments (Fig. 1c) [37], or more complex ordered arrangements [38–41].

These fluorite-like $[Ln_2O_2]^{2+}$ layers are also observed in ternary oxychalcogenides including the metastable *oA* polymorph of La_2O_2S which is formed from the topochemical anion deintercalation reaction of $La_2O_2S_2$ (Fig. 1e) [42]. $La_2O_2S_2$ is interesting in that the $[La_2O_2]^{2+}$ layers are separated by layers containing $(S_2)^{2-}$ dimer anions [43,44] leading to the possibility of topochemical redox reactions involving either the intercalation of a metal cation, or the deintercalation of sulfur [2,45]. The structural chemistry of $Ln_2O_2MQ_2$ (Q = S, Se) materials is rich with several different structure types (and polymorphism for several compositions) reported [46–48]; the possibility of targeting metastable phases and structures by topochemical intercalation reactions (that may not be accessed by high temperature reactions that favour thermodynamic products) [49–51] makes these topochemical redox reactions particularly exciting.

To date, most topochemical intercalation reactions into oxychalcogenides have focused on monovalent M^{+} cations [1,15,16] but Sasaki *et al.* have recently explored the topochemical reactions between

* Corresponding author.
E-mail address: emma.mccabe@durham.ac.uk (E.E. McCabe).

https://doi.org/10.1016/j.solidstatesciences.2024.107719
Received 16 July 2024; Received in revised form 30 September 2024; Accepted 7 October 2024
Available online 9 October 2024

$La_2O_2S_2$ and iron, cobalt and nickel [52]. XRD analysis of the bulk reaction products indicated that the reactions proceeded to give sulfur deintercalation products, but characterisation at shorter length scales by electron microscopy gave some evidence of M^{2+} (M = Fe, Ni) intercalation [52]. The precursor for our intercalation reactions is $La_2O_2S_2$ and Mvélé et al. have recently shown that by anion deintercalation, a metastable "*oA*" polymorph of La_2O_2S can be formed (Fig. 1), in contrast to the thermodynamically-stable "*hP*" polymorph. Both polymorphs adopt layered structures but differ in that *oA*-La_2O_2S is polar (with a pseudo-tetragonal crystal structure) whilst *hP*-La_2O_2S has a trigonal, centrosymmetric structure [42].

Our combined experimental and computational study reported here builds on the work of Sasaki *et al.* [52] and focuses on $M^{2+} = Zn^{2+}$, Sn^{2+} phases. $La_2O_2ZnSe_2$ has been prepared by high temperature solid state reaction and adopts the "intermediate" cation-ordered ZrCuSiAs-derived structure [37] (Fig. 1c) and we have considered synthetic routes to the oxysulfide analogue $La_2O_2ZnS_2$, and a hypothetical phase $La_2O_2SnS_2$ predicted to have a band gap well-matched to the solar spectrum (see supporting information). However, our experimental work indicates that binary and ternary phases are favoured over these quaternary oxysulfides for all reaction routes studied, consistent with recent work by Sasaki et al. for topochemical reactions with M = Fe, Co, Ni [52]. Computational work using density functional theory is used to explore this and highlights the challenges in preparing quaternary oxychalcogenides containing M^{2+} ions.

2. Methods

High temperature solid state reactions were carried out using stoichiometric quantities of La_2O_3 (Alfa Aesar, ≥99.9 %, pre-dried at 1000 °C for 12h before use), Zn (Alfa Aesar, −325 mesh, ≥99.9 %), Sn (ThermoScientific, −325 mesh, ≥99.8 %), S (Alfa Aesar, −325 mesh, ≥99.5 %), and Al powder (Alfa Aesar, −325 mesh, ≥99.5 %) acting as an oxygen-getter where appropriate. Metal powders were stored and manipulated inside a nitrogen-filled glovebox. Reagents were intimately ground by hand in an agate pestle and mortar. Sample mixtures were then placed in a small alumina crucible which was placed inside a quartz ampoule, evacuated and sealed. The sealed quartz ampoule was then heated at 2 °C min^{-1} to 400 °C, kept at this temperature for 12 h, then heated at 0.5 °C min^{-1} to 600 °C, kept at this temperature for 1 h, then

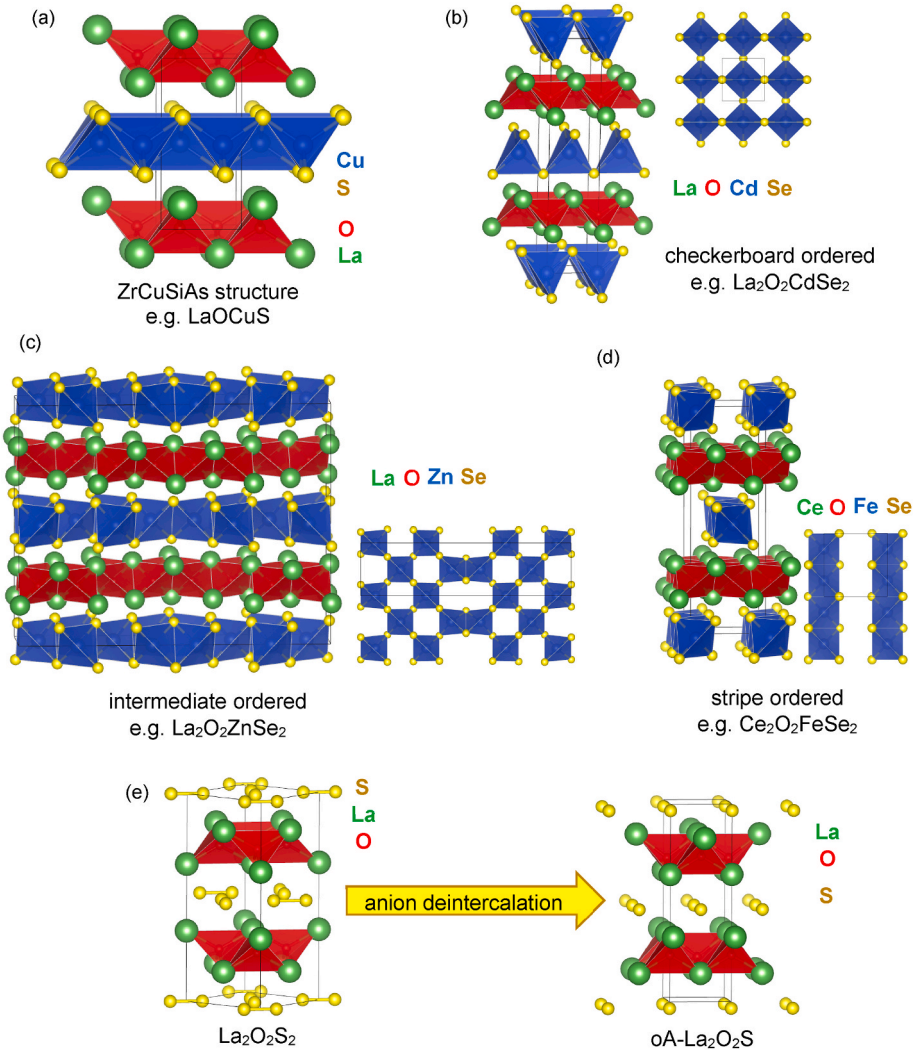

Fig. 1. (a) ZrCuSiAs structure as adopted by LaOCuS showing La, O, Cu and S ions in green, red, blue and yellow, and OLa_4 and CuS_4 tetrahedra in red and blue, respectively; panels (b)–(d) show ZrCuSiAs-derived cation-ordered structures including (b) checkerboard ordering as adopted by $La_2O_2CdSe_2$ [28] with La, O, Cd and Se ions in green, red, blue and yellow, and OLa_4 and $CdSe_4$ tetrahedra in red and blue, respectively; (c) shows intermediate ordered structure as adopted by $La_2O_2ZnSe_2$ [33] with La, O, Zn and Se ions in green, red, blue and yellow, and OLa_4 and $ZnSe_4$ tetrahedra in red and blue, respectively; (d) shows stripe ordered structure as adopted for one polymorph of $Ce_2O_2FeSe_2$ [31] with Ce, O, Fe and Se ions in green, red, blue and yellow, and OCe_4 and $FeSe_4$ tetrahedra in red and blue, respectively; (e) shows the metastable *oA* polymorph of La_2O_2S which can be formed by topochemical reaction from $La_2O_2S_2$ [38].

heated at 1 °C min^{-1} to the final reaction temperature and kept at this reaction temperature for 24 h. The final reaction temperatures (600–1100 °C for high temperature reactions, and 200 - 420 °C for topochemical reactions) are indicated on figures showing XRPD data (Figs. 2, 3 and 5).

Low temperature topotactic reactions using $La_2O_2S_2$ precursor were also carried out with Zn and Sn powders. $La_2O_2S_2$ was prepared (yellow powder, purity ≥85 % by mass, some *hP*-La_2O_2S impurity present) by reacting La_2S_3 (Strem Chemicals, 99.9%-La) with La_2O_3 (Alfa Aesar, ≥99.9 %, pre-dried at 1000 °C for 12h before use) and S (Alfa Aesar, −325 mesh, ≥99.5 %) at 700 °C for 48h twice with an intermediate grinding step, as reported previously [45]. The $La_2O_2S_2$ precursor was then reacted with stoichiometric amounts of Zn or Sn powders in evacuated, sealed quartz tubes, as described above, at reaction temperatures between 200 and 420 °C. Ball milling reactions were carried out using a Fritsch Pulverisette 6 Classic line planetary ball mill. 1.2 g of powder was placed in an 80 ml zirconia milling bowl with 25 zirconia milling balls (10 mm diameter) (19:1 ratio of milling media mass to sample mass) and milled in an N_2(g) atmosphere at 500 rpm.

Synthesis reactions were monitored using X-ray powder diffraction (XRPD) using a Rigaku Miniflex 600 with Cu Kα radiation (with Ni filter) operating in reflection mode. XRPD data were analysed using TopasAcademic software [53,54] for Rietveld refinements [55].

Diffuse-reflectance spectra were obtained using an OceanOptics DH-2000 deuterium light source and a Maya2000 Pro spectrometer equipped with a 50 mm diameter integrating sphere and OceanOptics' SpectraSuite software. NaCl was used as a reference. The diffuse reflectance *R* was measured from 200 to 1100 nm (1.13–6.20 eV) and then averaged over four measurements.

Selected area electron diffraction (SAED) and high resolution electron microscopy (HREM) data were collected using a Jeol 2100F transmission electron microscope operating at 200 keV. The sample was deposited onto a holey carbon grid. This was mounted in a double-tilt sample holder and zone-axis diffraction patterns were acquired using a Gatan Rio CMOS camera. Energy dispersive X-ray (EDX) data were collected with an Oxford Instruments X-Max 65T silicon drift detector.

Electronic structure calculations were carried out with *ab initio* density functional theory (DFT) using the plane-wave pseudopotential method implemented in the CASTEP code [56]. Calculations were carried out using the Perdew-Burke-Ernzerhof (PBE) exchange correlation functional [57] with a plane-wave cut-off energy of 1150 eV. The k-point spacing was decided by a Monkhorst-Pack grid [58] to give convergence of the total energy to a tolerance of ≤3 meV $atom^{-1}$. Geometry optimisations were converged to tolerances of: total energy (2 x 10^{-5} eV/atom), maximum ionic force (5 x 10^{-2} eV/Å), maximum ionic displacement (1 x 10^{-3} Å), and maximum stress component (0.1 GPa). For molecular species (O_2), one formula unit was placed in a sufficiently large cubic unit cell (*a* = 15 Å) to model a vacuum and experimentally-determined bond lengths were used in these initial molecular structures, used to calculate formation enthalpies of the oxide species. The reaction enthalpies ΔH_r were calculated from the formation enthalpies ΔH_f for reactants and products:

$$\Delta H_r = \sum \Delta H_f(product) - \sum \Delta H_f(reactant)$$

with formation enthalpies calculated from the relaxed total energies of each component and its constituent elements:

$$\Delta H_f = E_{total}(component) - \sum E_{total}(constituent\ elements).$$

The PBE exchange correlation functional is expected to slightly underestimate the formation energies calculated for these materials [59,60], and also to underestimate their band gaps [61]. The numerical error in the calculations is better than 3 meV per atom.

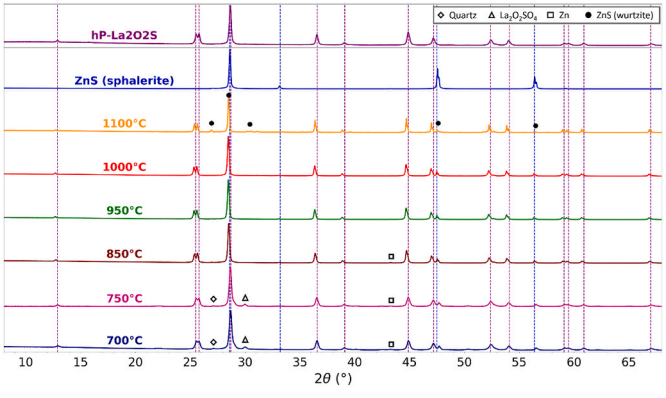

Fig. 2. XRPD patterns for high temperature reactions between La_2O_3, Zn, S and Al (as an oxygen-getter) following reaction Scheme 1. Reactions were carried out in evacuated and sealed quartz ampoules with reaction times of 24 h. Blue and purple vertical lines indicate main peak positions for ZnS (dark grey powder) and *hP*-La_2O_2S (white powder), respectively.

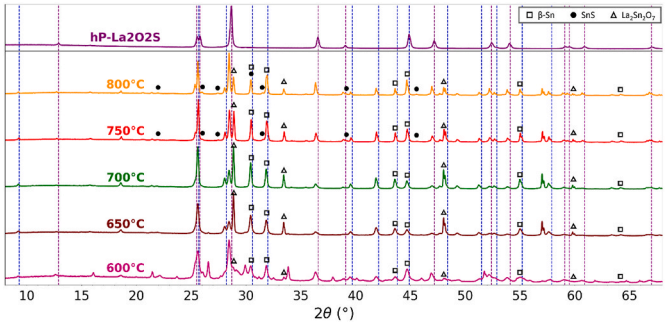

Fig. 3. XRPD patterns for high temperature reactions between La_2O_3, Sn, S and Al (as an oxygen-getter) following reaction Scheme 2. Reactions were carried out in evacuated and sealed quartz ampoules with reaction times of 24 h. Blue and purple vertical lines indicate main peak positions for $La_2O_2SnS_3$ and *hP*-La_2O_2S, respectively.

3. Results and discussion

A key observation from our combined experimental and computational study is the difficulty in preparing bulk $La_2O_2MQ_2$ phases (M^{2+}, *Q* = S, Se), consistent with the recent work of Sasaki *et al.* for M^{2+} = Ni^{2+}, Co^{2+}, Fe^{2+} [52]. We summarise below the results from our attempted synthesis using both high temperature solid state reactions as well as lower temperature topochemical reactions, and we discuss the insights from our computational work to explain the reaction outcomes.

3.1. High temperature solid state reactions of Zn^{2+} phases

Following the high temperature synthesis reported for $La_2O_2ZnSe_2$ [37], we attempted to prepare the quaternary oxysulfide $La_2O_2ZnS_2$ by a similar route. Our initial attempts involved direct reaction of La_2O_2S with ZnS with the hope of forming the quaternary phase $La_2O_2ZnS_2$. Reactions were carried out at 700 °C and at 1000 °C but no reaction between these reagents was observed by XRPD, instead the resulting samples contained only unreacted La_2O_2S and ZnS (see supporting information). Estimates of the reaction enthalpy (+0.485 eV, based on the formation energies of La_2O_2S, ZnS and $La_2O_2ZnS_2$) were consistent with this observation suggesting the reagents are more stable (at least at 0 K) than the quaternary phase.

Different reagents were then chosen, and from stoichiometric quantities of these reagents, two reaction paths can be considered (Scheme 1):

1a forming ternary and binary La_2O_2Q and Z*nQ* phases;

1b forming the quaternary oxychalcogenide $La_2O_2ZnQ_2$.

For a wide range of reaction temperatures (700–1100 °C), the

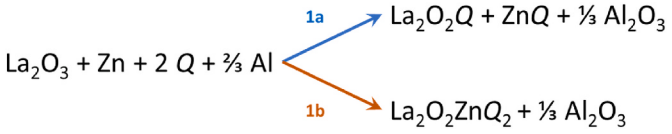

Scheme 1.

oxysulfide system was observed to follow route 1a forming only binary and ternary phases, with no traces of the quaternary $La_2O_2ZnS_2$ phase observed (Fig. 2).

This result contrasts with the La – O – Zn – Se system for which the quaternary phase $La_2O_2ZnSe_2$ was prepared at 1100 °C. DFT calculations were carried out to gain an insight into the different reactivities of these systems. Possible reaction paths and products were identified based on our experimental observations using XRPD analysis, and on literature reports of similar synthetic work.

Before calculating the reaction enthalpies for reaction routes 1a and 1b, geometry optimisations of the $La_2O_2ZnQ_2$ structures were carried out. For both Q = S and Se, the "intermediate" structure of *Cmce* symmetry was found to be the most stable of these cation-ordered structures (see SI, and consistent with experimental work on $La_2O_2ZnSe_2$[37]) and this structure was used in subsequent calculations.

Table 1 shows the calculated reaction enthalpies for both zinc oxychalcogenide systems for reaction routes 1a and 1b. Both routes are enthalpically favourable for both Q = S and Se, but route 1a (to give binary and ternary phases, and not the desired quaternary phase) is favoured over route 1b for both systems. However, there's very little enthalpic difference between these reaction routes for the oxyselenide system and so presumably other factors (including entropy considerations) favour the quaternary phase at the high reaction temperatures used in synthesis.

To understand the relative stabilities of the different reaction products, formation energies ΔH_f were calculated for the different components (Table 2). It's clear that the formation of Al_2O_3 for both reaction routes plays a role in driving both forward reactions. Although the formation energies for components in both systems are comparable, and particularly for the quaternary phases $La_2O_2ZnQ_2$, the slightly greater stability of the ternary La_2O_2S and binary ZnS tip the balance for the oxysulfide system, favouring reaction route 1a. The greater stability of these simpler systems for Q = S perhaps reflects the stronger bonding for the harder S^{2-} anion: the moderate charge density of the La^{3+} cation probably allows for stronger bonding in the ternary oxysulfide La_2O_2S than in the more covalent La_2O_2Se, and similarly for Zn^{2+} in ZnS compared with ZnSe (Mulliken charges calculated for Zn and Q in ZnQ were ±0.5 for Q = S compared with ±0.1 for Q = Se, reflecting the more ionic bonding for the sulfide compared with the selenide) (see Table 2).

3.2. High temperature solid state reactions of Sn phases

Experimental work was also carried out on the analogous tin system with the initial aim of preparing a quaternary Sn^{2+} phase $La_2O_2SnS_2$. The proposed Sn^{2+} oxysulfide was of interest because of the potential for the Sn^{2+} $5s^2$ lone pair to contribute to the top of the valence band, tuning the band gap towards the solar region as reported for other tin chalcogenides [62,63]. Indeed projected density of states from our electronic structure calculations for the more stable proposed $La_2O_2SnS_2$ structures

Table 1
Reaction enthalpies ΔH_r (eV) for reaction routes shown in Scheme 1 (uncertainties ~3 meV per atom).

ΔH_r (eV)	Q = S	Q = Se
Reaction 1a: $La_2O_2Q + ZnQ + {}^1/_3\ Al_2O_3$	−5.673	−5.085
Reaction 1b: $La_2O_2ZnQ_2 + {}^1/_3\ Al_2O_3$	−5.189	−4.924
Difference	0.484	0.161

Table 2
Formation enthalpies ΔH_f (eV per formula unit) for products shown in Scheme 1 (uncertainties ~3 meV per atom).

ΔH_f (eV per formula unit)	La_2O_2Q	ZnQ	$La_2O_2ZnQ_2$	Al_2O_3
Q = S	−16.076	−1.682	−17.273	−16.715
Q = Se	−15.736	−1.434	−17.008	−16.715

indicate hybridised Sn 5s and S 3p states contributing to the top of the valence band to give estimated band gaps ~0.7–1.3 eV (see SI).

Similar to the Zn systems described above, reaction paths giving Sn^{2+} products can be proposed for the Sn systems, as well as a reaction to give a quaternary Sn^{4+} phase $La_2O_2SnS_3$ (Scheme 2).

As for the proposed zinc oxysulfide $La_2O_2ZnS_2$, no traces of the proposed Sn^{2+} phase $La_2O_2SnS_2$ were observed over a range of reaction temperatures and instead the quaternary Sn^{4+} phase $La_2O_2SnS_3$ was formed via reaction route 2c, alongside binary and ternary phases formed via route 2a (Fig. 3). We note that the coefficients for 2c are underdetermined (five constants on the left, seven on right) therefore an additional constraint is needed which is taken from the weight percentages obtained from experiment. The competing phases in reaction 2c were identified from analysis of the XRPD data collected on samples from the 800 °C synthesis attempt.

Again, DFT calculations were carried out to explore the relative stabilities of the different reaction products (see Table 3 and 4). Geometry optimisation calculations for the proposed Sn^{2+} phases $La_2O_2SnQ_2$ indicated that the intermediate structure was the lowest energy model for Q = S, and within error, this model was lowest in energy (comparable with the checkerboard model) for Q = Se, and so the intermediate structure was used in subsequent calculations.

Analysis of XRPD data suggested the reaction formed phases in similar ratios to those suggested in reaction Scheme 2c, although the amount of pyrochlore $La_2Sn_2O_7$ decreased with further heating, suggesting that the ratios shown may not reflect the final reaction equilibrium. Nonetheless, there was no experimental evidence for the formation of the quaternary Sn^{2+} phase $La_2O_2SnS_2$. The lower stabilities of the quaternary Sn^{2+} phases $La_2O_2SnQ_2$ may reflect the larger size of the Sn^{2+} cations but also its preference for lower symmetry coordination environments due to the stereochemical activity of its lone pair: SnS (black powder) adopts a structure with Sn^{2+} cations in distorted trigonal based pyramidal sites/distorted tetrahedral sites with one apex vacant [64,65]. By contrast, Sn^{4+} ions are more comparable in size to other cations accommodated by ZrCuSiAs-related structures (ionic radii of four-coordinate ions are 0.55 Å and 0.60 Å for Sn^{4+} and Cu^{+} ions, respectively) [66], and with their $5s^0$ electron configuration, they have no electronic driving force for lower symmetry coordination environments. The Sn^{4+} cation can be accommodated within a sulfide layer between $[La_2O_2]^{2+}$ blocks with a slight change to stoichiometry for charge balance to give $La_2O_2SnS_3$ with chains of corner-linked SnS_4 tetrahedra [67].

3.3. Computational study of high temperature reactions to form $La_2O_2Cu_2Q_2$ (Q = S, Se) and comparison with M^{2+} systems

Quaternary LaOCuS and LaOCuSe phases (with Cu^{+} cations fully occupying the tetrahedral sites within the chalcogenide layers) have

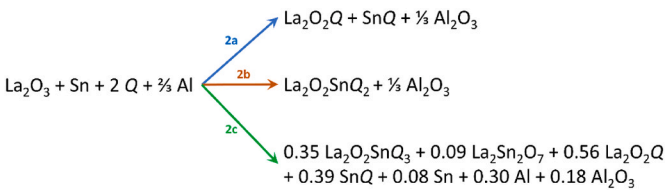

Scheme 2.

Table 3
Reaction enthalpies ΔH_r (eV) for reaction routes shown in Scheme 2 (uncertainties ~3 meV per atom).

ΔH_r (eV)	Q = S	Q = Se
Reaction 2a: $La_2O_2Q + SnQ + {}^1/_3\ Al_2O_3$	−4.989	−4.579
Reaction 2b: $La_2O_2SnQ_2 + {}^1/_3\ Al_2O_3$	−4.107	−3.998
Reaction 2c: 0.35 $La_2O_2SnQ_3$ + 0.09 $La_2Sn_2O_7$ + 0.56 La_2O_2Q + 0.39 SnQ + 0.08 Sn + 0.30 Al + 0.18 Al_2O_3	−3.631	−3.195

been prepared successfully via several high temperature reactions [68,69] (Scheme 3). DFT calculations for the monovalent Cu^+ systems give some insights into the difficulties in preparing analogous M^{2+} (M = Zn, Sn) systems by high temperature reactions as discussed above. For ease of comparison with the M^{2+} cation-ordered systems described above, the doubled formula $La_2O_2Cu_2Q_2$ will be used (see Table 6).

Calculated reaction enthalpies (Table 5) indicate that all reaction paths in Schemes 3 and 4 are enthalpically favourable. As expected, reactions to give Al_2O_3 as a product (routes 4a and 4b) are more favourable. These results suggest that although the quaternary phase $La_2O_2Cu_2Q_2$ might be favoured for Q = Se, the two routes are comparable for Q = S. Experimentally the quaternary phase $La_2O_2Cu_2Q_2$ can be prepared for both Q = S, Se by high temperature reaction routes, suggesting that choice of synthesis temperature might tune other factors not included in our model (including entropy terms) to allow the synthesis of pure $La_2O_2Cu_2S_2$.

Formation enthalpies for reactions 4a and 4b were calculated (Table 6) for comparison with analogous reactions in Schemes 1 and 2.

As for the Zn systems (Table 2), the greater stability of the Q = S phases compared with Q = Se phases is seen. Comparing the divalent Zn^{2+} system with the monovalent Cu^+ system discussed here indicates comparatively weaker bonding for Cu_2Q phases compared with ZnQ. The stronger bonding in MQ phases (such as ZnS) with M^{2+} ions probably contributes to the greater difficulty in synthesising quaternary ZrCuSiAs phases with divalent M^{2+} ions compared with the binary and ternary products, in contrast to the monovalent M^+ systems.

3.4. *Topochemical reactions to form $La_2O_2M_xQ_2$ ($M = Zn^{2+}$, Sn^{2+} for x = 1; $M = Cu^+$ for x = 2)*

Our experimental and computation work above illustrate the challenges in preparing quaternary ZrCuSiAs phases with M^{2+} ions by high temperature reactions, with binary and ternary products often favoured over quaternary phases on enthalpic grounds. Low temperature topochemical reactions can allow access to metastable phases, avoiding preparation of thermodynamically favoured products [49]. Sasaki et al. have shown the potential of $La_2O_2S_2$ (containing S_2^{2-} dimer anions) to undergo low temperature topochemical reactions [2], including intercalation of Cu^+ ions to form $La_2O_2Cu_2S_2$ [1]. These redox reactions involve oxidation of a metal reactant (e.g. Rb, Ag, Ni, Cu) to drive the reduction of S_2^{2-} anions to sulfide S^{2-} anions: $S_2^{2-} + 2e^- \rightarrow 2\ S^{2-}$. The challenge is that these topochemical reactions can proceed either by S deintercalation (for example to form metastable oA-$La_2O_2S_{1.5}$ or oA-La_2O_2S) [2], or via metal intercalation (e.g. to form $La_2O_2Cu_2S_2$, isostructural with that prepared by high temperature reactions) as illustrated in Fig. 4 [1].

We carried out topochemical reactions of $La_2O_2S_2$ with Zn and with Sn between 200 and 420 °C and found that for these M^{2+} ions, deintercalation reactions are favoured, forming binary and ternary products and not the quaternary phases (Fig. 5), consistent with results from reactions with Rb, Ag and Ni (see summary in Fig. 4) [2]. In our reactions with Sn, the metastable oA polymorph of La_2O_2S is formed for reactions between 360 and 380 °C, whilst the thermodynamically stable hP polymorph is observed at higher temperatures. These low temperature topochemical reactions should be under kinetic control but our reactions with $La_2O_2S_2$ don't proceed below ~360–400 °C, significantly higher in temperature than solid state topochemical reactions with Cu [1]. This indicates a higher activation barrier for these topochemical reactions – perhaps reflecting a particle size issue with our reactants, or a higher activation barrier to intercalation of the more highly charged divalent

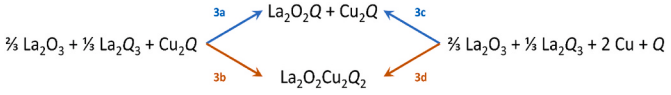

Scheme 3.

Table 5
Reaction enthalpies ΔH_r (eV) for reaction routes shown in Schemes 3 and 4 (uncertainties ~3 meV per atom).

ΔH_r (eV)	Q = S	Q = Se
Reaction 3a: $La_2O_2Q + Cu_2Q$	−0.806	−0.757
Reaction 3b: $La_2O_2Cu_2Q_2$	−0.781	−1.229
Reaction 3c: $La_2O_2Q + Cu_2Q$	−1.272	−0.739
Reaction 3d: $La_2O_2Cu_2Q_2$	−1.247	−1.211
Reaction 4a: $La_2O_2Q + Cu_2Q + {}^1/_3\ Al_2O_3$	−4.458	−3.634
Reaction 4b: $La_2O_2Cu_2Q_2 + {}^1/_3\ Al_2O_3$	−4.433	−4.106

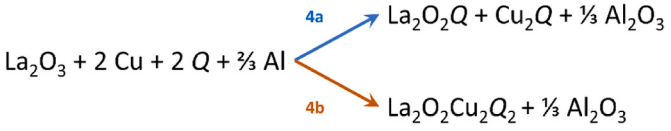

Scheme 4.

Table 6
Formation enthalpies ΔH_f (eV per formula unit) for products shown in Scheme 4 (uncertainties ~3 meV per atom).

ΔH_f (eV)	La_2O_2Q	Cu_2Q	$La_2O_2Cu_2Q_2$	Al_2O_3
Q = S	−16.076	−0.466	−16.517	−16.715
Q = Se	−15.736	0.018	−16.190	−16.715

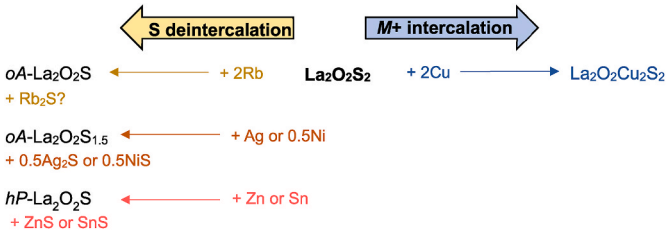

Fig. 4. Schematic summarising outcomes of topochemical reactions with Cu [1], Rb, Ag or Ni [2,3], or with Zn or Sn described here.

Table 4
Formation enthalpies ΔH_f (eV per formula unit) for reagents and products shown in Scheme 2 (uncertainties ~3 meV per atom).

ΔH_f (eV per formula unit)	La_2O_2Q	SnQ	$La_2O_2SnQ_2$	$La_2O_2SnQ_3$	$La_2Sn_2O_7$	Al_2O_3
Q = S	−16.076	−0.998	−16.192	−17.370	−31.190	−16.715
Q = Se	−15.736	−0.928	−16.082	−16.745	−31.190	−16.715

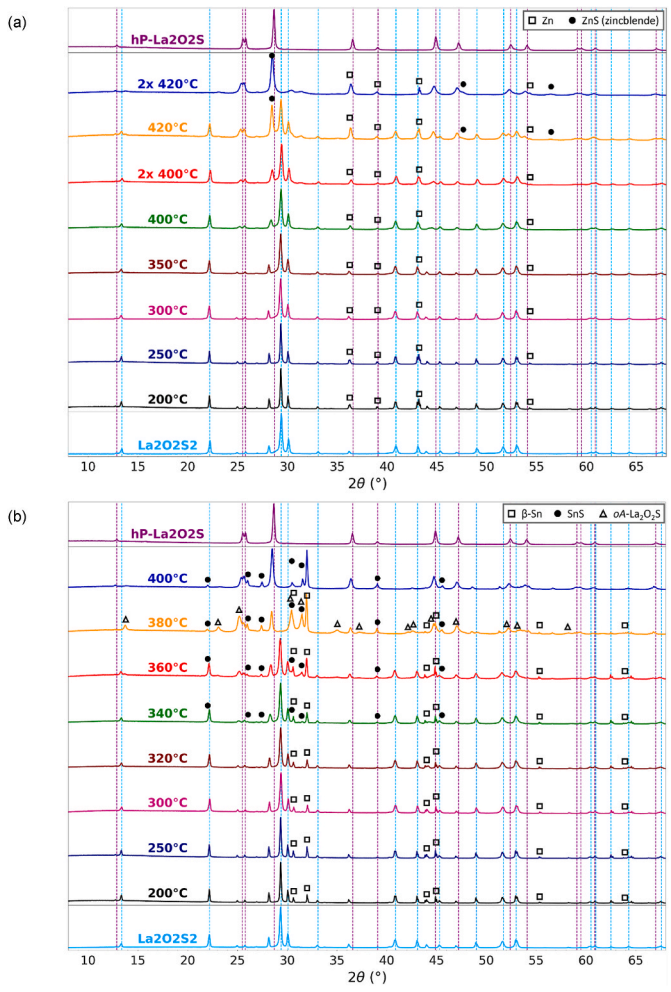

Fig. 5. XRPD patterns for low temperature topochemical reactions between $La_2O_2S_2$ and (a) Zn or (b) Sn. Reactions were carried out in evacuated and sealed quartz ampoules with reaction times of 18 h. Cyan and purple vertical lines indicate main peak positions of $La_2O_2S_2$ and *hP*-La_2O_2S phases, respectively.

cations.

Whilst preparing this manuscript we became aware of the recently reported topochemical reactions between $La_2O_2S_2$ and Fe, Co or Ni [52]. Although electron microscopy work suggested some inclusions or intergrowths of M – S phases (M = Fe, Ni), XRPD analysis indicated that, at least in terms of the bulk products, these reactions favour sulfur deintercalation. This is consistent with our observations of reactions with Zn and Sn.

Selected area electron diffraction and HREM imaging were also carried out on a sample from the topochemical reaction between $La_2O_2S_2$ and Zn at 420 °C to look for any evidence of Zn intercalation over short length scales as reported by Sasaki et al. for M = Fe, Ni [52]. EDX data taken at various parts of our sample indicated regions of La-O-S phases as well as ZnS regions. Electron diffraction data collected at various points were consistent with the *hP*-La_2O_2S ($P\bar{3}m1$ symmetry) phase, and in places with $La_2O_2SO_4$. HREM images showed evidence of small crystallites with spacings consistent with binary or ternary phases such as $La_2O_2SO_4$ (see supporting information). These microscopy results suggest that even at short length scales there is no evidence for successful intercalation reactions with Zn^{2+} ions, consistent with the bulk characterisation using XRPD.

It has already been reported that topochemical reactions can be limited by particle size [70] and its possible that the higher activation barrier to ionic mobility of the more highly charged M^{2+} ions is a limiting factor in preparing bulk $La_2O_2MS_2$ (M^{2+}) phases by topochemical routes. This should be partly mitigated by the solvothermal reaction method followed by Sasaki *et al.* for Ni reaction [52], but it would be interesting to see whether ball milling of the topochemical reaction mixtures prior to heating to reaction temperatures might give further M^{2+} intercalation. Our own ball milling reaction of $La_2O_2S_2$ precursor (prepared by high temperature reactions) and Zn suggested the formation of La_2O_2S, consistent with the high temperature topochemical reactions described above (see SI).

4. Conclusions

Our combined experimental and computational study of $La_2O_2MQ_2$ phases with divalent M^{2+} cations illustrates the challenges in synthesising this family of oxychalcogenides. Not only are the size and coordination preference of the M cations critical factors, but also the subtle balance in stabilities of binary and ternary phases formed via competing reactions. It is surprising that the quaternary oxyselenide $La_2O_2ZnSe_2$ can be prepared relatively easily [37], yet we were unable to prepare the analogous oxysulfide $La_2O_2ZnS_2$ in this work, presumably due the subtle difference in stabilities of the La_2O_2Q and ZnQ phases versus the quaternary $La_2O_2ZnQ_2$ phases (Q = S, Se). Attempts to overcome some of these thermodynamic constraints to prepare metastable phases by topochemical routes were also unsuccessful; the mobility of M^{2+} ions (compared with lower charge density M^{+} ions) may be a limiting factor, and it would be interesting to explore the role of particle size in these reactions.

CRediT authorship contribution statement

Glen R. Hebberd: Investigation, Formal analysis, Data curation. **Stewart J. Clark:** Supervision, Methodology. **Emma E. McCabe:** Writing – original draft, Supervision, Funding acquisition, Conceptualization.

Declaration of competing interest

The authors declare that they have no known competing financial interests or personal relationships that could have appeared to influence the work reported in this paper.Professor Stewart J. Clark, Mr Glen R. Hebberd, Dr Emma E. McCabe reports some financial support, administrative support, and equipment, supplies were provided by Durham University. Mr Glen R. Hebberd reports financial support was provided by Engineering and Physical Sciences Research Council. If there are other authors, they declare that they have no known competing financial interests or personal relationships that could have appeared to influence the work reported in this paper.

Acknowledgements

This work was supported by the Engineering and Physical Sciences Research Council (grant number EP/S023836/1) as part of the ReNU CDT. We are grateful to John S. O. Evans and Ivana R. Evans for sealing line and glove box access. We thank Matthew Dyer, Laurent Cario and Isabelle Braems for helpful discussions. We are grateful to the Royal Society for equipment grant RG130844.

Appendix A. Supplementary data

Supplementary data to this article can be found online at https://doi.org/10.1016/j.solidstatesciences.2024.107719.

Data availability

No data was used for the research described in the article.

References

[1] S. Sasaki, G. Steciuk, C. Guillot-Deudon, M.T. Caldes, I. Braems, E. Janod, B. Corraze, S. Jobic, L. Cario, Solvothermal and mechanochemical intercalation of Cu into La2O2S2 enabled by the redox reactivity of (S2)2− pairs, Dalton Trans. 50 (36) (2021) 12419–12423.

[2] S. Sasaki, M.T. Caldes, C. Guillot-Deudon, I. Braems, G. Steciuk, L. Palatinus, E. Gautron, G. Frapper, E. Janod, B. Corraze, S. Jobic, L. Cario, Design of metastable oxychalcogenide phases by topochemical (de)intercalation of sulfur in La2O2S2, Nat. Commun. 12 (1) (2021) 3605.

[3] S.D.N. Luu, P. Vaqueiro, Layered oxychalcogenides: structural chemistry and thermoelectric properties, Journal of Materiomics 2 (2) (2016) 131–140.

[4] X.L. Shi, J. Zou, Z.G. Chen, Advanced thermoelectric design: from materials and structures to devices, Chem. Rev. 120 (15) (2020) 7399–7515.

[5] I.E. Castelli, T. Olsen, Y. Chen, Towards photoferroic materials by design: recent progress and perspectives, J. Phys.: Energy 2 (1) (2020) 011001.

[6] Z. Liang, C.F. Yan, S. Rtimi, J. Bandara, Piezoelectric materials for catalytic/photocatalytic removal of pollutants: recent advances and outlook, Applied Catalysis B-Environmental 241 (2019) 256–269.

[7] H. Kageyama, K. Hayashi, K. Maeda, J.P. Attfield, Z. Hiroi, J.M. Rondinelli, K. R. Poeppelmeier, Expanding frontiers in materials chemistry and physics with multiple anions, Nat. Commun. 9 (2018).

[8] K. Maeda, F. Takeiri, G. Kobayashi, S. Matsuishi, H. Ogino, S. Ida, T. Mori, Y. Uchimoto, S. Tanabe, T. Hasegawa, N. Imanaka, H. Kageyama, Recent progress on mixed-anion materials for energy applications, Bull. Chem. Soc. Jpn. 95 (1) (2022) 26–37.

[9] S. Tippireddy, D.S.P. Kumar, S. Das, R.C. Mallik, Oxychalcogenides as thermoelectric materials: an overview, ACS Appl. Energy Mater. 4 (3) (2021) 2022–2040.

[10] Y.J. Zhang, H.P. Wu, Z.G. Hu, H.W. Yu, Oxychalcogenides: a promising class of materials for nonlinear optical crystals with mixed-anion groups, Chem.–Eur. J. 29 (17) (2023).

[11] Y.F. Shi, W.B. Wei, X.T. Wu, H. Lin, Q.L. Zhu, Recent progress in oxychalcogenides as IR nonlinear optical materials, Dalton Trans. 50 (12) (2021) 4112–4118.

[12] G.G. Zhang, X.C. Wang, Oxysulfide semiconductors for photocatalytic overall water splitting with visible light, Angewandte Chemie-International Edition 58 (44) (2019) 15580–15582.

[13] A. Ishikawa, T. Takata, J.N. Kondo, M. Hara, H. Kobayashi, K. Domen, Oxysulfide Sm2Ti2S2O5 as a stable photocatalyst for water oxidation and reduction under visible light irradiation (lambda <= 650 nm), J. Am. Chem. Soc. 124 (45) (2002) 13547–13553.

[14] Q. Wang, M. Nakabayashi, T. Hisatomi, S. Sun, S. Akiyama, Z. Wang, Z.H. Pan, X. Xiao, T. Watanabe, T. Yamada, N. Shibata, T. Takata, K. Domen, Oxysulfide photocatalyst for visible-light-driven overall water splitting, Nat. Mater. 18 (8) (2019) 827. +.

[15] S. Giri, S. Dey, E. Suard, S.J. Clarke, Sr2MnO2Na1.6Se2: a metamagnetic layered oxychalcogenide synthesized by reductive Na intercalation to break [Se2]2- perselenide dimer units, Chem. Mater. 36 (11) (2024) 5730–5740.

[16] S. Sasaki, S.J. Clarke, S. Jobic, L. Cario, Anionic redox topochemistry for materials design: chalcogenides and beyond, ACS Organic & Inorganic Au 4 (1) (2024) 26–40.

[17] S.A. Bacha, S. Saitzek, E.E. McCabe, H. Kabbour, Photocatalytic and photoconduction response under visible light of the lone pair based oxysulfide Sr6Cd2Sb6O7S10, Inorg. Chem. 61 (2022) 18611–18621.

[18] S. Al Bacha, S. Saitzek, P. Roussel, M. Huvé, E.E. McCabe, H. Kabbour, Low carrier effective masses in photoactive Sr2Sb2O2Q3 (Q = S, Se): the role of the lone pair, Chem. Mater. 35 (22) (2023) 9528–9541.

[19] R.Q. Wang, F. Liang, F.K. Wang, Y.W. Guo, X. Zhang, Y. Xiao, K.J. Bu, Z.S. Lin, J. Y. Yao, T.Y. Zhai, F.Q. Huang, Sr6Cd2Sb6O7S10: strong SHG response activated by highly polarizable Sb/O/S groups, Angewandte Chemie-International Edition 58 (24) (2019) 8078–8081.

[20] R. Wang, F. Wang, X. Zhang, X. Feng, C. Zhao, K. Bu, Z. Zhang, T. Zhai, F. Huang, Improved polarization in the Sr6Cd2Sb6O7Se10 oxyselenide through design of lateral sublattices for efficient photoelectric conversion, Angew. Chem. Int. Ed. 61 (33) (2022) e202206816.

[21] S.J. Clarke, P. Adamson, S.J.C. Herkelrath, O.J. Rutt, D.R. Parker, M.J. Pitcher, C. F. Smura, Structures, physical properties, and chemistry of layered oxychalcogenides and oxypnictides, Inorg. Chem. 47 (19) (2008) 8473–8486.

[22] M. Orr, G.R. Hebberd, E.E. McCabe, R.T. Macaluso, Structural diversity of rare-earth oxychalcogenides, ACS Omega 7 (10) (2022) 8209–8218.

[23] F. Li, J.F. Li, L.D. Zhao, K. Xiang, Y. Liu, B.P. Zhang, Y.H. Lin, C.W. Nan, H.M. Zhu, Polycrystalline BiCuSeO oxide as a potential thermoelectric material, Energy Environ. Sci. 5 (5) (2012) 7188–7195.

[24] J. Li, J.H. Sui, Y.L. Pei, C. Barreteau, D. Berardan, N. Dragoe, W. Cai, J.Q. He, L. D. Zhao, A high thermoelectric figure of merit $ZT > 1$ in Ba heavily doped BiCuSeO oxyselenides, Energy Environ. Sci. 5 (9) (2012) 8543–8547.

[25] Y. Liu, L.D. Zhao, Y.C. Liu, J.L. Lan, W. Xu, F. Li, B.P. Zhang, D. Berardan, N. Dragoe, Y.H. Lin, C.W. Nan, J.F. Li, H.M. Zhu, Remarkable enhancement in thermoelectric performance of BiCuSeO by Cu deficiencies, J. Am. Chem. Soc. 133 (50) (2011) 20112–20115.

[26] C. Zhang, J. He, R. McClain, H. Xie, S. Cai, L.N. Walters, J. Shen, F. Ding, X. Zhou, C.D. Malliakas, J.M. Rondinelli, M.G. Kanatzidis, C. Wolverton, V.P. Dravid, K. R. Poeppelmeier, Low thermal conductivity in heteroanionic materials with layers of homoleptic polyhedra, J. Am. Chem. Soc. 144 (6) (2022) 2569–2579.

[27] A. Chaupatnaik, A.M. Abakumov, G. Rousse, D. Foix, J. Louis, B.T. Leube, J.-M. Tarascon, Electrochemical exploration of layered Cu-based oxychalcogenides obtained topochemically via anionic redox and displacement reaction, Chem. Mater. 35 (15) (2023) 5924–5935.

[28] K. Ueda, S. Inoue, S. Hirose, H. Kawazoe, H. Hosono, Transparent p-type semiconductor: LaCuOS layered oxysulfide, Appl. Phys. Lett. 77 (17) (2000) 2701–2703.

[29] Z.A. Ren, W. Lu, J. Yang, W. Yi, X.L. Shen, Z.C. Li, G.C. Che, X.L. Dong, L.L. Sun, F. Zhou, Z.X. Zhao, Superconductivity at 55K in iron-based F-doped layered quaternary compound Sm $O_{1-x}F_x$ FeAs, Chin. Phys. Lett. 25 (6) (2008) 2215–2216.

[30] H. Takahashi, K. Igawa, K. Arii, Y. Kamihara, M. Hirano, H. Hosono, Superconductivity at 43 K in an iron-based layered compound Lao1-xFxFeAs, Nature 453 (7193) (2008) 376–378.

[31] I. Ijjaali, K. Mitchell, C.L. Haynes, A.D. McFarland, R.P. Van Duyne, J.A. Ibers, Synthesis, crystal structure, and optical properties of CeMn0.5OSe, J. Solid State Chem. 176 (1) (2003) 170–174.

[32] H. Hiramatsu, K. Ueda, T. Kamiya, H. Ohta, M. Hirano, H. Hosono, Optical properties and two-dimensional electronic structure in wide-gap layered oxychalcogenide: La2CdO2Se2, J. Phys. Chem. B 108 (45) (2004) 17344–17351.

[33] H. Hiramatsu, K. Ueda, T. Kamiya, H. Ohta, M. Hirano, H. Hosono, Synthesis of single-phase layered oxychalcogenide La2CdO2Se2: crystal structure, optical and electrical properties, J. Mater. Chem. 14 (19) (2004) 2946–2950.

[34] I.Y. Baranov, V.A. Dolgikh, B.A. Popovkin, Phase relations in the La2O2X-MX (M=Zn, Cd, Hg; X=S, Se) systems: structure of a new cadmium lanthanum oxoselenenide, Zh. Neorg. Khim. 41 (11) (1996) 1916–1919.

[35] E.E. McCabe, D.G. Free, J.S.O. Evans, A new iron oxyselenide Ce2O2FeSe2: synthesis and characterisation, Chem. Commun. 47 (4) (2011) 1261–1263.

[36] E.E. McCabe, C. Stock, J.L. Bettis, M.H. Whangbo, J.S.O. Evans, Magnetism of the Fe2+ and Ce3+ sublattices in Ce2O2FeSe2: a combined neutron powder diffraction, inelastic neutron scattering, and density functional study, Phys. Rev. B 90 (23) (2014) 235115.

[37] A.J. Tuxworth, E.E. McCabe, D.G. Free, S.J. Clark, J.S.O. Evans, Structural characterization and physical properties of the new transition metal oxyselenide La2O2ZnSe2, Inorg. Chem. 52 (4) (2013) 2078–2085.

[38] S. Peschke, F. Nitsche, D. Johrendt, Flux synthesis, modulated crystal structures, and physical properties of REMn0.5SeO (RE = La, Ce), Z. Anorg. Allg. Chem. 641 (3–4) (2015) 529–536.

[39] C.M. Ainsworth, C.-H. Wang, H.E. Johnston, E.E. McCabe, M.G. Tucker, H.E. A. Brand, J.S.O. Evans, Infinitely adaptive transition-metal ordering in Ln2O2MSe2-type oxychalcogenides, Inorg. Chem. 54 (15) (2015) 7230–7238.

[40] C.H. Wang, C.M. Ainsworth, D.Y. Gui, E.E. McCabe, M.G. Tucker, I.R. Evans, J.S. O. Evans, Infinitely adaptive transition metal oxychalcogenides: the modulated structures of Ce2O2MnSe2 and (Ce0.78La0.22)(2)O2MnSe2, Chem. Mater. 27 (8) (2015) 3121–3134.

[41] S. Peschke, D. Johrendt, The modulated structures of La2–xPrxO2MnSe2 ($0 \leq x \leq 1$) and La2–xNdxO2MnSe2 ($0 \leq x \leq 0.6$), Z. für Kristallogr. - Cryst. Mater. 231 (2) (2016) 89–95.

[42] L.-B. Mvélé, S. Sasaki, P. Deniard, Y. Tsujimoto, E. Janod, C. Guillot-Deudon, M. T. Caldes, I. Braems, B. Corraze, S. Jobic, L. Cario, Synthesis of non-centrosymmetric, metastable rare-earth oxysulfides by anionic redox topochemistry, Chem. Mater. 35 (18) (2023) 7597–7604.

[43] L.-B. Mvélé, S. Sasaki, C. Latouche, P. Deniard, E. Janod, I. Braems, S. Jobic, L. Cario, Revisiting the crystal structure of layered oxychalcogenides Ln2O2S2 (Ln = La, Pr, and Nd), Inorg. Chem. 62 (19) (2023) 7264–7272.

[44] J. Ostoréro, M. Leblanc, Room-temperature structure of La2O2S2, Acta Crystallographica Section C: Crystal Structure Communications 46 (8) (1990) 1376–1378.

[45] S. Sasaki, D. Driss, E. Grange, J.-Y. Mevellec, M.T. Caldes, C. Guillot-Deudon, S. Cadars, B. Corraze, E. Janod, S. Jobic, L. Cario, A topochemical approach to synthesize layered materials based on the redox reactivity of anionic chalcogen dimers, Angew. Chem. Int. Ed. 57 (41) (2018) 13618–13623.

[46] S. Peschke, V. Weippert, A. Senyshyn, M.J. Mühlbauer, O. Janka, R. Pöttgen, S. Holenstein, H. Luetkens, D. Johrendt, Flux synthesis, crystal structures, and magnetic ordering of the rare-earth chromium(II) oxyselenides RE2CrSe2O2 (RE = La–Nd), Inorg. Chem. 56 (4) (2017) 2241–2247.

[47] S. Peschke, D. Johrendt, Flux synthesis, crystal structures, and magnetism of the series La2n+2MnSen+2O2n+2 (n = 0–2), Inorganics 5 (1) (2017) 9.

[48] F. Nitsche, R. Niklaus, D. Johrendt, New polymorphs of RE2FeSe2O2 (RE = La, Ce), Z. Anorg. Allg. Chem. 640 (14) (2014) 2897–2902.

[49] J. Gopalakrishnan, Chimie douce approaches to the synthesis of metastable oxide materials, Chem. Mater. 7 (7) (1995) 1265–1275.

[50] R. Uppuluri, A. Sen Gupta, A.S. Rosas, T.E. Mallouk, Soft chemistry of ion-exchangeable layered metal oxides, Chem. Soc. Rev. 47 (7) (2018) 2401–2430.

[51] M.A. Hayward, Topochemical reactions of layered transition-metal oxides, Semicond. Sci. Technol. 29 (6) (2014).

[52] S. Sasaki, D. Driss, M.T. Caldes, E. Gautron, S. Cadars, E. Janod, B. Corraze, C. Guillot-Deudon, I. Braems, S. Jobic, L. Cario, Microscopic evidences for intercalation of nickel and iron into layered oxysulfide La2O2S2, Solid State Sci. 147 (2024) 107383.

[53] A.A. Coelho, Topas Academic: General Profile and Structure Analysis Software for Powder Diffraction Data, Bruker AXS, Karlsruhe, Germany, 2012.

[54] A. Coelho, TOPAS and TOPAS-Academic: an optimization program integrating computer algebra and crystallographic objects written in C++, J. Appl. Crystallogr. 51 (1) (2018) 210–218.

[55] H. Rietveld, A profile refinement method for nuclear and magnetic structures, J. Appl. Crystallogr. 2 (2) (1969) 65–71.

[56] S.J. Clark, M.D. Segall, C.J. Pickard, P.J. Hasnip, M.I.J. Probert, K. Refson, M. C. Payne, First principles methods using CASTEP, Z. für Kristallogr. - Cryst. Mater. 220 (5–6) (2005) 567–570.
[57] J.P. Perdew, K. Burke, M. Ernzerhof, Generalized gradient approximation made simple, Phys. Rev. Lett. 77 (18) (1996) 3865–3868.
[58] H.J. Monkhorst, J.D. Pack, Special points for Brillouin-zone integrations, Phys. Rev. B 13 (12) (1976) 5188–5192.
[59] G. Hautier, S.P. Ong, A. Jain, C.J. Moore, G. Ceder, Accuracy of density functional theory in predicting formation energies of ternary oxides from binary oxides and its implication on phase stability, Phys. Rev. B 85 (15) (2012) 155208.
[60] S. Lany, Semiconductor thermochemistry in density functional calculations, Phys. Rev. B 78 (24) (2008) 245207.
[61] P. Borlido, T. Aull, A.W. Huran, F. Tran, M.A.L. Marques, S. Botti, Large-scale benchmark of exchange–correlation functionals for the determination of electronic band gaps of solids, J. Chem. Theor. Comput. 15 (9) (2019) 5069–5079.
[62] A. Walsh, G.W. Watson, Influence of the anion on lone pair formation in Sn(II) monochalcogenides: a DFT study, J. Phys. Chem. B 109 (40) (2005) 18868–18875.
[63] L.A.H. Jones, W.M. Linhart, N. Fleck, J.E.N. Swallow, P.A.E. Murgatroyd, H. Shiel, T.J. Featherstone, M.J. Smiles, P.K. Thakur, T.-L. Lee, L.J. Hardwick, J. Alaria, F. Jäckel, R. Kudrawiec, L.A. Burton, A. Walsh, J.M. Skelton, T.D. Veal, V. R. Dhanak, Sn 5s2 lone pairs and the electronic structure of tin sulphides: a photoreflectance, high-energy photoemission, and theoretical investigation, Phys. Rev. Mater. 4 (7) (2020) 074602.
[64] S. Del Bucchia, J.-C. Jumas, M. Maurin, Contribution a l'etude de composes sulfures d'etain(II): affinement de la structure de SnS, Acta Crystallogr. B 37 (10) (1981) 1903–1905.
[65] J. Breternitz, R. Gunder, H. Hempel, S. Binet, I. Ahmet, S. Schorr, Facile bulk synthesis of π-cubic SnS, Inorg. Chem. 56 (19) (2017) 11455–11457.
[66] R.D. Shannon, Revised effective IONIC-radii and systematic studies of interatomic distances in halides and chalcogenides, Acta Crystallogr. A 32 (SEP1) (1976) 751–767.
[67] S. Benazeth, M. Guittard, P. Laruelle, Structure de l'oxysulfure de lanthane et d'etain (LaO)4Sn2S6, Acta Crystallogr. C 41 (5) (1985) 649–651.
[68] H. Hiramatsu, H. Yanagi, T. Kamiya, K. Ueda, M. Hirano, H. Hosono, Crystal structures, optoelectronic properties, and electronic structures of layered oxychalcogenides MCuOCh (M = Bi, La; Ch = S, Se, Te): Effects of electronic configurations of M3+ ions, Chem. Mater. 20 (1) (2008) 326–334.
[69] K. Ueda, H. Hosono, Band gap engineering, band edge emission, and p-type conductivity in wide-gap LaCuOS1−xSex oxychalcogenides, J. Appl. Phys. 91 (7) (2002) 4768–4770.
[70] Z. Liang, M. Amano Patino, M. Hendrickx, J. Hadermann, M.A. Hayward, Microstructural activation of a topochemical reduction reaction, ACS Organic & Inorganic Au 2 (1) (2022) 75–82.